Transactions of the Missouri Academy of Science

A Comparative Study to Quantify Sensitive Dependence in Numerical Models for a Developing Low in the Southern Plains

Amy E. Schnetzler[1], Justin M. Glisan[1], H. Athar[1,2], Patrick S. Market[1], and Anthony R. Lupo[1],*

[1]Department of Soil, Environmental, and Atmospheric Science, 302 Anheuser Busch Natural Resources Building, University of Missouri – Columbia, Columbia, MO 65211
[2]Center of Excellence for Climate Change Research, King Abdulaziz University, P.O. Box 80208, Jeddah 21589, Saudi Arabia
*Corresponding author address: Dr. Anthony Lupo, Dept. of Soils, Environmental and Atmospheric Sciences, University of Missouri, 302E ABNR Building, Columbia, MO 65211
Email: lupoa@missouri.edu

A Comparative Study to Quantify Sensitive Dependence in Numerical Models for a Developing Low in the Southern Plains

Amy E. Schnetzler[1], Justin M. Glisan[1], H. Athar[1,2], Patrick S. Market[1], and Anthony R. Lupo[1,]*

[1]Department of Soil, Environmental, and Atmospheric Science, 302 Anheuser Busch Natural Resources Building, University of Missouri – Columbia, Columbia, MO 65211
[2]Center of Excellence for Climate Change Research, King Abdulaziz University, P.O. Box 80208, Jeddah 21589, Saudi Arabia
*Corresponding author address: Dr. Anthony Lupo, Dept. of Soils, Environmental and Atmospheric Sciences, University of Missouri, 302E ABNR Building, Columbia, MO 65211
Email: lupoa@missouri.edu

Abstract: *Studies have shown that numerical models display the characteristics of chaotic systems, and that the solutions can be sensitive to the initial conditions, the model used, or the parameterizations used. Using the Kain-Fritsch, Grell, and modified Kuo convective parameterizations in the MASS and the WRF model, the results from a case study show that 48-h forecasts were not identical. Lyapunov exponents were calculated by plotting forecast trajectories in a phase diagram and estimating the rate of trajectory divergence for two time periods outside the study of the main cyclone. These calculations did show divergence at a rate which was consistent with differences in model height in 48-h forecasts from other studies. Additionally, the integrated enstrophy can be used to estimate the Lyapunov value. Finally, a qualitative analysis comparing various model runs (pseudo-ensemble) was performed to determine if there were regions or areas where consistent differences in the runs existed between the indexes used for forecasting convective precipitation. Results demonstrated that the region of the southeast United States associated with the developing cyclone showed the most significant differences in these indexes and for heights and temperatures. The differences in the model forecasts between convective parameterizations (intramodel forecasts) in this case were not as great as the model-to-model forecast differences (intermodel forecasts).*

Introduction

A chaotic system can behave as if it contains elements of predictability, as well as elements of "randomness" [1,2] such that only statistical prediction would be possible. Several studies have shown that numerical models possess these elements, to some degree, and these include sensitive dependence on the initial conditions and a low degree of internal memory. As such, the predictability within our physical system decreases the further one is from the initial time step.

In an effort to examine the numerical stability of the forecast models, a quantity known as the Lyapunov Exponent [3] was employed in evaluating the time evolution of the model. The study of trajectory stability contains a powerful tool, in that the use of the exponent also can provide a diagnostic which quantifies the predictability within the system [4,5]. Lyapunov exponents mathematically arise from the eigenvalue-solutions to the differential equations representing a physical system. In the simplest of terms, the exponent itself describes the time-averaged rate of change of convergence (or divergence) of nearby trajectories in a system. Since these entities are solutions to eigenvectors, there can be as many exponents as there are dimensions of a physical system. In a system in which the sum of the Lyapunov exponents is negative, the system would exhibit a high degree of predictability. In other words, the trajectories within the phase space would converge (as time approaches infinity) towards an attractor. This attractor is located somewhere in the center of the so-called "basin of attraction" [5]. It should be noted here that this work will not attempt to equate predictability and deterministic behavior [6].

The numerical models used to generate forecasts are sensitive to their initial conditions. These models use differential equations to form their dynamic core, and here we will assume that these models, given the parameterizations used and with the same initial conditions will uniquely evolve toward one solution in time [6]. Initial conditions that are similar, however,

can produce very different results because of factors such as the numerical methods employed or the physical schemes used. There have been many investigations in the literature using this strategy [7,8]. In these studies, the varied initial conditions varied were those related to the moist convection schemes in order to investigate the impact of moist baroclinic processes. It has been found that the error growth in a control run is approximately 36 hours [8], and that error growth is a function of moist instability.

A model can be used such that the parameters described in the model are identical except for one condition, the convective parameterization scheme employed, such as; the Kain-Fritsch [9], Grell [10,11], Betts-Miller-Janjic [12,13] or a modified Kuo scheme (e.g., see [14]). In generating a model ensemble, this one difference in parameterizations can cause the final output of each run to differ from each other even though the initial conditions are the same. This is one strategy that will be employed in this study (intramodel comparison), and these results will be compared to model-to-model differences (intermodel comparison).

Through this study of model behaviors, it will be demonstrated that the generated forecasts from the numerical models indeed possess a degree of chaotic behavior, and the solutions are not identical. This can be quantified simply by examining the values of some commonly used stability indexes (such as the total totals index (TT), convective available potential energy (CAPE), and the K-index (KI)), as well as the areal extent of the convective precipitation, and we will use these simple methods here. Our study will also examine the utility of some simple methods for quantifying the Lyapunov exponent using values readily obtained from the model. Section 2 describes the models, data, and the methods used. Section 3 will compare the results among convective schemes, between different models, and predictability. Section 4 will state the major conclusions.

Model Descriptions, Data, and Methods

The GFS Model

For a case study beginning 09 November 2006, the ensemble forecast solutions of the Global Forecast System (GFS) model over Missouri were used to estimate the Lyapunov exponents as an indicator of chaos in weather forecasting. The GFS was built upon the Medium Range Forecast model (MRF) [15].

The operational GFS forecast model is a high-resolution global spectral model. In the horizontal, the resolution is spectral triangular truncation 170 (T170), which corresponds to a 512 by 256 Gaussian grid, roughly equivalent to 0.7 by 0.7 degrees latitude / longitude grid spacing. The vertical coordinate is an unequally spaced sigma coordinate. This includes 42 vertical sigma levels extending through a column from the surface to roughly 2.0 hPa. The GFS dynamic core is a primitive equation model using vorticity, divergence, surface pressure (ln[psfc]), specific humidity and virtual temperature as the dependent variables. A more detailed description of the GFS model can be obtained from a NOAA website (http://www.emc.ncep.noaa.gov/gmb/moorthi/gam.html) and references found therein. Output from the GFS model is available operationally through the National Center for Environmental Prediction and is archived locally in the University of Missouri weather and computer center located within the atmospheric sciences program. This model can provide upper air variables output such as geometric height (z), temperature (T), specific humidity (q), and u,v wind components.

The NCEP operational GEFS is GFS-based (http://www.emc.ncep.noaa.gov/gmb/ens/), and the daily forecasts are available via this website. The data can be accessed via anonymous FTP and is stored in GRIB format. The software needed to unpack the data is also available through this site. Briefly, the NCEP EFS consists of a 17-member ensemble (at 0000 UTC) which includes 2 control runs, 10 perturbed forecasts, and 5 forecasts from the previous 1200 UTC cycle. The rationale for the development and formulation of the NCEP EFS and/or a description of the system are found on the above site as well as in the peer-reviewed literature [16,17,18,19].

The essential atmospheric physics is included in the GFS via the spectral transform method of the primitive equations. In this class of models, the values of all state variables are available in both spectral and grid point domains at each time step. More importantly, convection occurs in the GFS when the cloud work function exceeds a certain threshold using the Grell scheme [11]. Mass flux of the cloud is determined using a quasi-equilibrium assumption based on this threshold cloud work function.

The MASS Model

Some of the model output was taken from simulations with the Mesoscale Atmospheric Simulation System (MASS) [20], version 6.0.1. This software build is a limited-area, hydrostatic, mesoscale numerical weather prediction model with a 44-km grid spacing and 26 vertical levels, formulated in x,y,σ-coordinates with the primitive equation set. In order to attempt a full accounting of all processes in the atmosphere, some assumptions and parameterizations became necessary. Specific parameterizations included a 1½ order closure scheme for the planetary boundary layer along with Grell, modified Kuo, and modified Kain-Fritsch cumulus parameterization schemes (in three different runs). Additional studies with the MASS platform can be found in the existing literature [20]. Also, the MASS model is proprietary (Meso, Inc.) and further information about the model, which is run in-house at the University of Missouri, can be found at http://www.meso.com/mass-user/masshome.htm. Further, three versions of the MASS model were employed here, namely the Kain-Fritsch (MASS4KF) or (A), Grell (MASS4GR) or (B), and Kuo-Mesoscale (or modified Kuo - MASS4KM) or (C). These three different convective schemes are available through the MASS model and will provide an opportunity to test the impact of using different convective schemes with the sae model and initial conditions.

The WRF Model

The Weather Research and Forecasting (WRF) Model is a next-generation mesoscale numerical weather prediction system designed to serve both operational forecasting and atmospheric research needs. In this particular case, the model is run operationally on a RedHat Linux workstation featuring a cold-start run every six hours, initialized on 12-km grid files from the North American Mesoscale (NAM) Model. No other data assimilation was used in these runs. The outer domain covered the continental United States with a grid spacing of 39 km with a nested 13-km domain centered over the central U.S. (Fig. 1). Both domains are given 31 levels in the hybrid sigma-isentropic coordinate system, which conforms to natural terrain near the surface and better defines boundary layer processes.

In a hydrostatic environment, the Grell [10,11] convective scheme was used for both outer and inner domains with two-way nesting. Also used was a microphysics scheme [21] which takes into effect graupel and ice particles in cloud processes. WRF allows researchers the ability to conduct simulations reflecting either real data or idealized configurations.

The WRF model is a fully compressible, non-hydrostatic model (with a hydrostatic option). The WRF maintains a selection of vertical coordinates to use, but the default is a hybrid isentropic-sigma coordinate system. The hybrid coordinate field allows for a better depiction of systems aloft with the ability of Θ coordinates to handle the location and intensity of frontal boundaries and also tropopause undulations. The use of σ coordinates, a terrain following coordinate system, provides a more homogenous view of observations than quasi-horizontal surfaces.

Methodologies

In this study, two methods were employed in an effort to analyze the differences that each ensemble model produced for

Figure 1.   View of the continental U.S. with white lines showing domain borders for WRF model runs. The model was run operationally every 6 hours. Domain 01 is every 39-km with the nested domain 02 every 13-km.
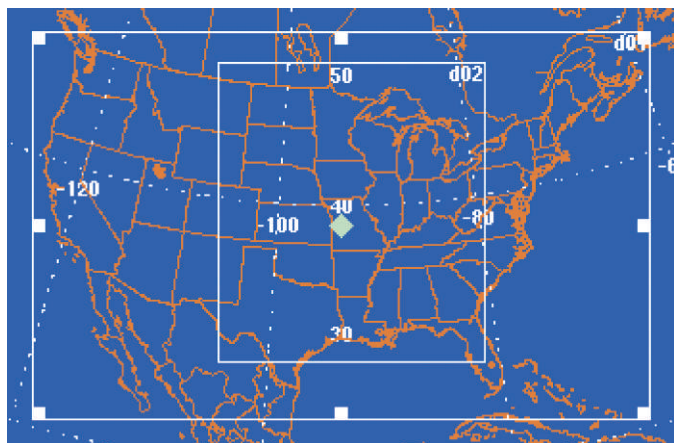
each of the forecasted events (i.e. 1200 UTC 26–0000 UTC 28 October 2006, 9–14 November 2006, and 13–18 November 2006). A more detailed study of the stability will be examined in the 1200 UTC October case (Fig. 2). This case was chosen because the developing low was prominent in the study region and became a rapidly developing low outside the area. While the system was developing in the southern plains of the United States during 26 October (Fig, 2a, and 2b), it was not an explosively developing cyclone (see [14]), and it moved slowly eastward. The following day, the cyclone reached the occlusion stage (Fig. 2c) and began to move northeastward (Fig. 2d). By the following day, the cyclone moved into the northeast United States (Fig. 2e), and then finally over the Canadian Maritimes (Fig. 2f). The two November time periods were examined in order to determine the degree of predictability within the models in randomly chosen time periods close to our case study. Additionally, there were no well-defined features in the study region during these two November periods. The synoptic observations for all three of these time periods were examined using the NOAA Daily Weather Maps site (http://www.hpc.ncep. noaa.gov/dailywxmap). In the November cases, an observational analysis was performed followed by a discussion of the calculation of Lyapunov exponents.

Model Output

The basis of this approach was a visual analysis of each forecast period for the MASS and WRF models. Given that only the convective term varied in each of the three MASS models, the control set of conditions and variables were created and used as the standard for each run performed by the two models (i.e., MASS and WRF).

For each model, geopotential heights and temperatures were plotted at initialization (0000 UTC 24 October), and then run for 48-h with 12-h iterations over the time period (Fig. 3, 0000 UTC 26 October). The three MASS and WRF variations were overlaid upon each other for visual error analysis. For each forecast time, isohypses and isotherms were analyzed visually. Perturbations in the individual fields, as well as, differences between each of the three model-derived fields were noted. While most runs produced a very similar result, there were some differences between the location of the trough and whether or not a close low developed. The second part of the analysis involved comparing each of the three MASS model variations with respect to where only the convective precipitation fell (Fig. 4) and, in turn, diagnosing the convective indexes and the relative degrees of percent error between each model.

Further diagnoses of the convective parameters were accomplished using skew T–log-P diagrams from four sites. Two locations were upstream (Topeka, Kansas (KTOP) and Fort Worth, Texas (KFWD)) of the convective event and two were downstream (Nashville, Tennessee (KBNA), Wilmington, Ohio (KILN)). Data derived from observed soundings were compared to those using forecast soundings from the MASS and WRF model. Model soundings were produced every six

Figure 2a–f.   Observational data obtained from Unisys for October 26, 27, and 28, 2006 for 00Z and 12Z time periods.
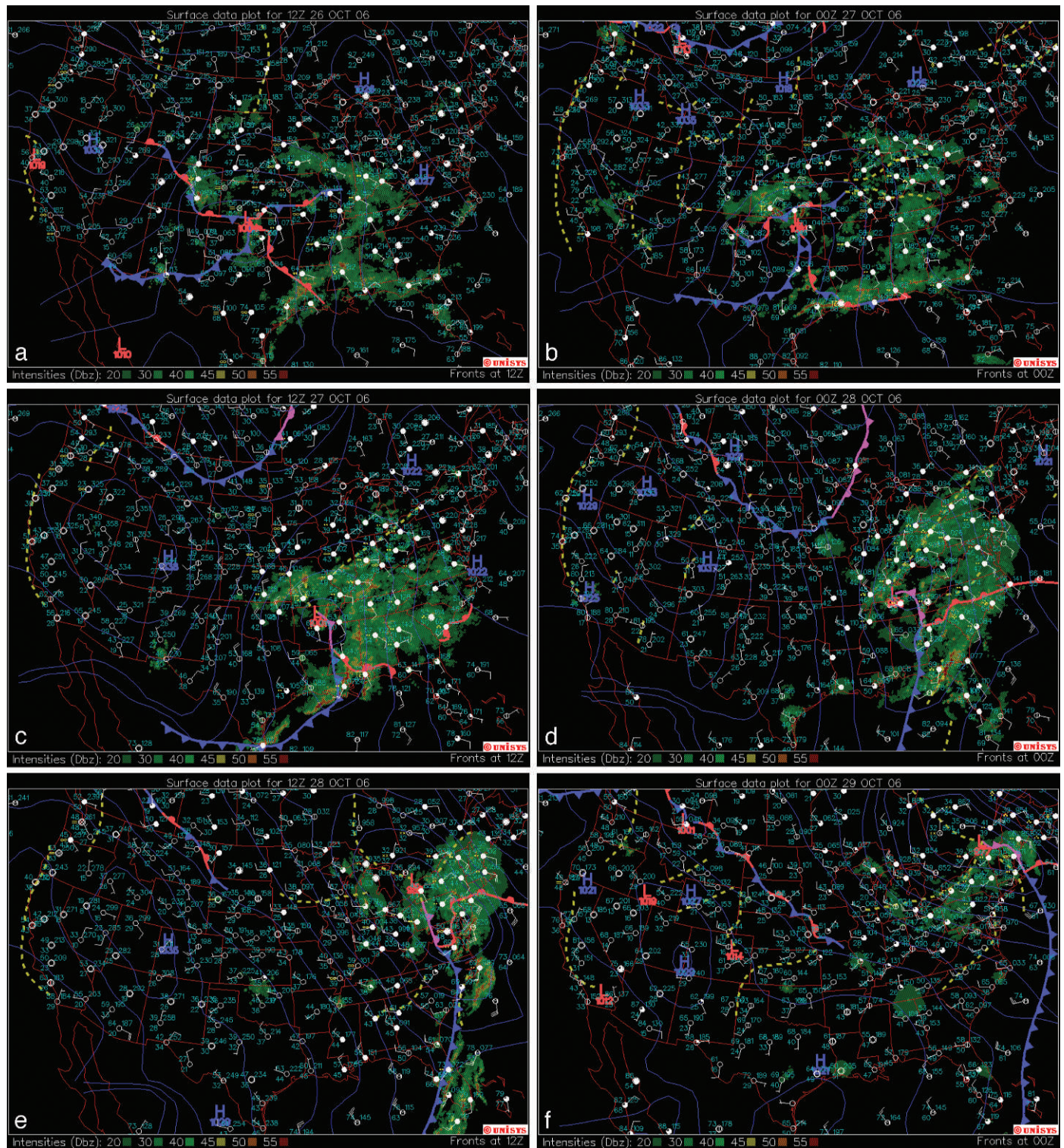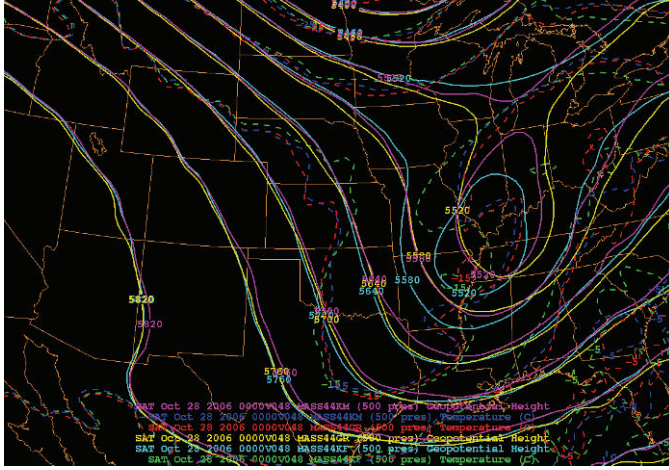
Figure 3. View of the last iteration of Geopotential Heights at the pressure level 500 hPa. The three schemes differ on the placement of the closed low.

hours, starting at 1200 UTC on 26 October 2006 through 0000 UTC on 28 October 2006. Analysis was limited to three well-known parameters, that of the KI, CAPE, TT, which were chosen for their simplicity. All three stability indices are used commonly to diagnose the possibility of thunderstorms, and generally appear on computer generated visualizations of soundings. Increasing values of each index also indicate a greater possibility that convective events will be severe. The values for each index were computed (Table 1).

The Stability Indices Used

The KI is simply a stability index that measures thunderstorm potential (probability) based on temperature lapse rate, moisture content of the lower troposphere, and the vertical extent of the moist layer [22]. This index can be calculated using the following equation:

$$KI = \left(T_{850hPa} - T_{500hPa}\right) - Td_{850hPa} - \left(T_{700hPa} - Td_{700hPa}\right), \quad (1),$$

where T is the temperature (°C) and T_d is the dewpoint temperature (°C). The second stability criterion used in this study was Convective Available Potential Energy (CAPE). Convection tends to be more vigorous with higher values of this quantity [22]. In this case, CAPE was calculated using the most unstable parcel, via the equation below:

$$CAPE = \int_{p_n}^{p_l} \left(\alpha_p - \alpha_l\right) dp, \quad (2),$$

where the specific volume of the parcel is denoted by α_p, and α_e is the specific volume of the environment. The final stability index used, the Total Totals, is a more general criterion. As values of TT increase, so does the probability of convective activity. When a value is greater than 50 is obtained, thunderstorm activity has a high probability of being severe. This index is a combination of two indices (vertical totals [VT] and cross totals [CT]) and is calculated by the following:

$$TT = VT + CT = T_{850hPa} + T_{d\,850hPa} - 2T_{500hPa},$$

where,

$$VT = T_{850hPa} - T_{500hPa} \quad \& \quad CT = T_{d\,850hPa} - T_{500hPa}. \quad (3),$$

Estimation of Lyapunov Exponents and Time Horizons

To give a quantitative measure of the sensitivity of the GFS ensemble to initial conditions, an estimate of the largest Lyapunov exponent (λ) of the system was made from forecasts of the events of 9–14 November 2006 and 13–18 November 2006. These time periods were chosen because they did not contain strong developing features or coherent features, which might be expected to exhibit a greater degree of predictability [5,8,23]. For each event, a control trajectory, as well as ten GFS ensemble trajectories, was analyzed for 120 h, and these represent the data archived here. The GFS was used for this analysis because the data were readily available and provided a large sample size. To obtain an approximate value for the largest Lyapunov exponent of a system, a N-dimensional Euclidean metric (N=165 for our data – or 500 hPa height data within our study area) was used to gauge the degree of divergence of discrete data points in the above time periods. The height data was discretized every six hours in the initial 24-h time period, then every 12 hours for the next 48-h interval, and finally every 24 hours for the last 48-h interval. At each verification time the distance of each ensemble trajectory from the control trajectory was calculated according to our metric. By plotting the data on a log-log plot and then calculating the slope of the linear regression line, the largest Lyapunov exponent was determined.

Analysis and Results

Lyapunov Values

The average of the largest exponents from individual ensemble trajectories for each event was calculated to be $\lambda = 0.22$ ($\lambda = 0.19$) for the 9–14 November 2006 (13–18 November 2006). These values ($\lambda > 0$) indicate that the model should display characteristics of chaotic systems, and that means forecasts may be unreliable after a certain time period (the e-folding time), or could give very different interpretations for the output (if calculating indexes). These values are consistent with regionally accumulated values of enstrophy, which [4] showed could be used to indicate flow stability as well. Then, [24] and [25] used this diagnostic to examine the stability of coherent anticyclonic vorticies called blocking events. They found that the regionally accumulated enstrophy was an effective tool for identifying the onset and termination of blocking, but was relatively small during the maintenance phase of the events. This calculation is relatively straightforward and can be computed using:

$$\sum \lambda_+ = \int_A \varsigma_r^2 dA \approx \sum_A \varsigma_r^2 \Delta x \Delta y \quad (4),$$

Figure 4.   The a) second and b) iteration of the 12-hour Convective Precipitation shows a) that the models began to disagree on areas of precipitation after one time period, and b) greater disagreement between all three schemes of the MASS.
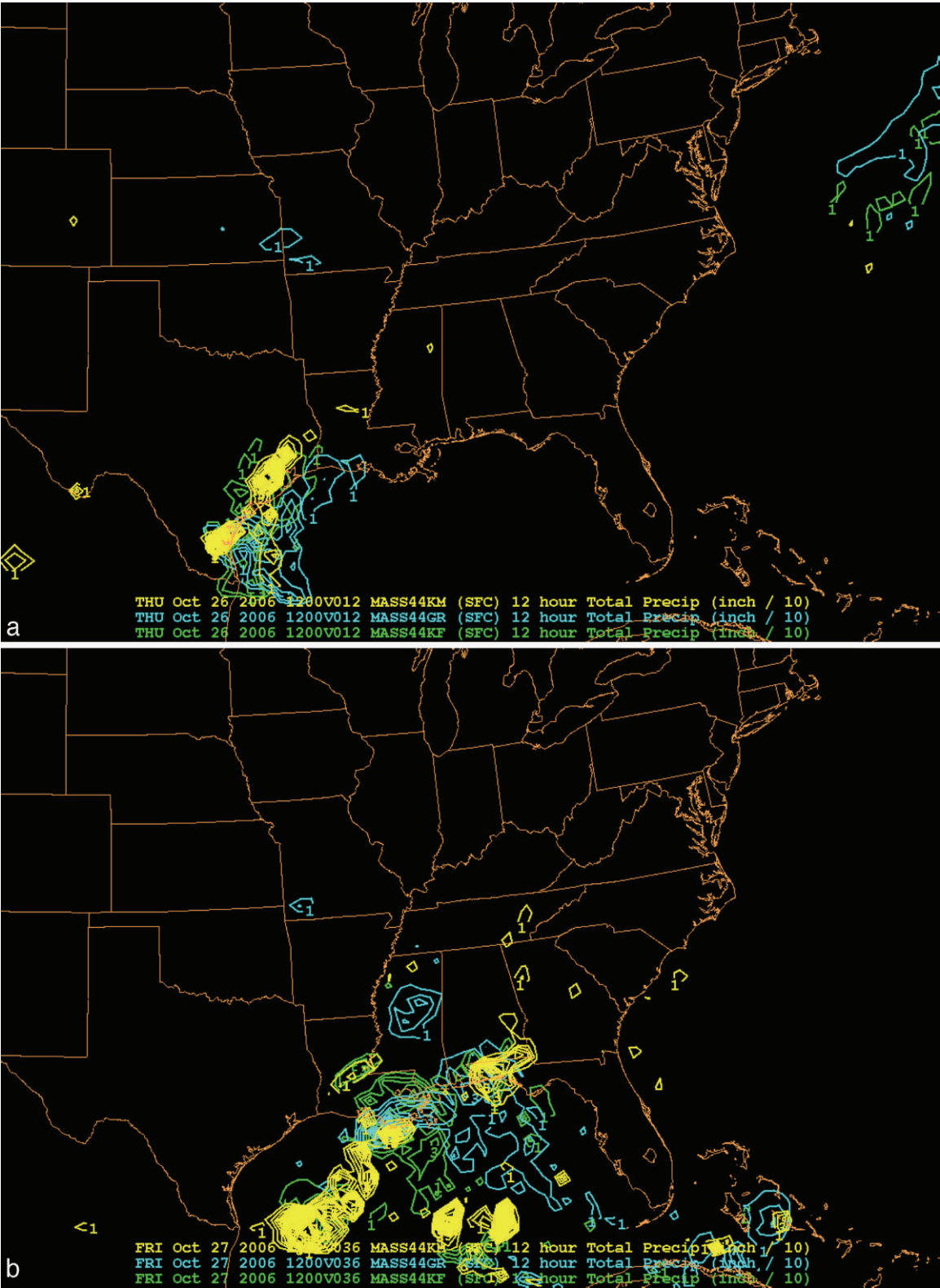
Table 1. The critical values for the stability indexes used here.

K-Index (KI)

> 0–18 = Stable, no thunderstorms
> 19–20 = Marginally unstable, thunderstorms unlikely
> 21–25 = Moderately unstable, isolated thunderstorms
> 26–30 = Widely scattered thunderstorms
> 31–35 = Numerous thunderstorms
> 36–40 = Very Unstable, thunderstorms very likely
> 40+ = Extremely unstable, 100% chance of thunderstorms

Convective Available Potential Energy (CAPE)

> <300 = Stable
> 300–1000 = Marginally unstable
> 1000–2500 = Moderately unstable
> 2500–3000 = Very unstable
> 3000–5000+ = Extremely unstable

Total Totals (TT)

> 45–50 = Possible thunderstorms
> 50–55 = Thunderstorms more likely, possibly severe
> 55–60 = Severe thunderstorms likely

in a gridded data set. As an example, the above expression can be calculated using a typical value for vorticity in the model field $|\varsigma_{rl}|=1.0 \times 10^{-5}$ s^{-1} and 40 km as the grid spacing (similar to our mesoscale models above), which yield a point value of 0.16. This is a value that is consistent with those above.

For a system with at least one positive Lyapunov exponent there is an associated time horizon beyond which prediction fails. The time horizon is known to be (from differential equations (for example [26]) and assuming this process is analogous to exponential decay or a Markov process):

$$\tau =(1/\lambda)* \ln (\text{tolerance/uncertainty}) \qquad (5),$$

where τ is time in hours. Thus, this value can easily be calculated using Eq. (4) and some reasonable estimates of tolerance and uncertainty.

In the models and observations, the uncertainty of the initial conditions was approximately 1% (or 0.01) or less for measuring height at 500 hPa (e.g., [27]). We can define *tolerance* as a good forecast, which should be a value larger than the uncertainty. Here we chose 10 m since it is as large or larger than the uncertainty, and a round number on the same scale as that of the analysis interval (60 m, see Fig. 3). Given the above estimate of the Lyapunov exponents from the GFS, the time horizon for an accurate prediction (within ten meters at 500 hPa) should be 31.4 and 36.4 hours, respectively. Using the estimate from Eq. (4) yields a time horizon of 43.2 hours, which is a little longer than those found graphically. However, these values are consistent with predictability values found in [7] (approximately 72 h) and [8] (about 36 h) using the NCAR Mesoscale Model (MM5 version 2).

Examining Eqs. (4) and (5) should reveal that even if tolerance were increased to 60 m, the graphical calculation of

predictability would be 39.5 and 45.8 hours, respectively, and from Eq. (4) yields 54.4 hours. This means that given our definition of tolerance, predictions should be useful within the time frame of the model runs (generally 48 hours). For the use of the convective indexes used below, 48 h would be a reasonable value. Additionally, the time horizon could be calculated quickly to estimate the reliability of model forecasts. Alternatively, an analysis of the output of (4) from a model forecast would suggest that a stronger vorticity field or decreased horizontal resolution would degrade the forecastability of these models. Conversely, a weaker vorticity field or increased horizontal resolution would improve model forecasts.

26–27 October 2006 Intra-Model Comparisons

As previously discussed, the MASS model was used by varying the three convective model parameterizations discussed in section 2 to demonstrate sensitivity to initial conditions. The model was initialized during 26–27 October 2006 in 12-h increments over 48 hours. These runs were compared with observational data obtained from Unisys (http://weather.unisys.com/archive/sfc_map/) versus the model runs in the domain shown in Fig. 1. Each parameterization was analyzed to ascertain if any one contained less error than the others.

In comparing the observational data to model prediction, the error increased following each of the successful time iterations for the three parameters. For example, the region of convective precipitation for the initialization agreed closely to the observations (not shown). As the verification time reached 12 hours, there was slightly less correspondence between the model runs and the observed data for the precipitation. In the 12-h run, shown in Fig. 4a (compare to Fig 2a), all models seem to slightly over-estimate the area of convective precipitation in the Texas-Gulf of Mexico region. By the 24-h run, the Kain-Fritsch and Kuo-Mesoscale parameterizations were forecasting an area of convective precipitation in southeastern Kansas that matched up well with the observed data. However, the area near the Gulf of Mexico has been over-estimated once again by all three parameters. For the 36-h (Fig. 4b) and 48-h runs, there was a noticeable change in that the models begin to pick up on smaller areas of convective precipitation that do not correspond to the observed data. Recall that our time horizon was on the order of 36-h in section 3.1, when using the MM5 or the GFS, and this seems to be the time horizon for the MASS here. In the 36-h and 48-h runs, the Kuo-Mesoscale parameter indicated convective precipitation off the coast of Florida where observed convection did not exist. Fig. 3 displays the geopotential heights and temperatures at 500-hPa. Model agreement is very poor in the region of low pressure for both parameters, but reasonable outside our domain.

Thus, from analyzing this case, it can be concluded that the MASS model system is sensitive to the initial conditions via the convective parameterization used and as a consequence, shows some of the characteristics of a chaotic system. However, what has not been determined is whether or not one of the convective

parameters represents a better forecasting parameterization, as all three did not match up perfectly with the observed data. A study of which one works better is beyond the scope of this study, and has been performed by others. However, as our study demonstrates, model forecast performance, and model agreement, can be relatively poor in a weaker cyclone event.

26–27 October 2006 Model-to-Observation Differences using Convective Indexes

The study above showed that there were some key differences between the forecasts of 500 hPa heights and temperatures as well as the convective precipitation. The production of precipitation depends on a couple of ingredients including the stability of the atmosphere, and as such we look at the stability at four different points within the domain. These cities were chosen in order to sample a geographically wide array of points and capture different points in the cyclone lifecycle. We can examine here what kind of information a forecaster at these four locations would have had to consider during the time of this event. The percent difference for the forecast index (KI, TT) was calculated for each variation of the MASS model and the WRF model in the four observation sites. The raw values are displayed in Tables 2–5 and summarized in Fig. 5. Fig. 5 contains the mean percent difference for each model-to-model comparison. Tables 2–5 show that occasionally there were percent differences above 500% since the actual forecast values (not shown) were relatively small. Also, due to a significant number of zero values, CAPE was not used in the model-to-model comparisons. Each MASS parameterization (A,B,C) was compared to one another in combination, and then each MASS model run was compared to the WRF model. The goal was to determine which is more important, the difference in convective parameterization or the use of a different model.

The three versions of the MASS model produced values that were similar to each other and generally provide the same interpretation regarding the probability of precipitation and its distribution, including the timing of the possible convection and its severity. The WRF model, however, produced raw higher values of TT than the MASS model at the downstream location (ILM) which indicated higher instability. But, in general the raw KI values were lower for the WRF. Thus, the implication was that the MASS (WRF) model would produce weaker (stronger), but more widespread (scattered) convective elements. At TOP and FWD, however, TT's were generally lower for both TT and KI in the WRF. The TTs indicated the possibility of thunderstorms at TOP early in the period. The overall interpretation was that the WRF did not predict a strong possibility of widespread convection. Again, there were more differences between the two models than there were between the three different convective schemes run in the MASS model.

Topeka and Fort Worth tended to have higher percent differences for TT while Nashville and Wilmington had lower values (Fig. 5). The models had the greatest differences at 0600 UTC 27 October (see Tables 2–5). Looking at the errors for KI,

Table 2. Actual values of CAPE, TT, and KI for 6-h time periods at KTOP beginning with 1200 UTC 26 October 2006 and ending with 0000 UTC 28 October 2006 (left), and % difference for the TT and KI for each model run. The formula is: | [(model1 – model 2) / model 2] * 100 |.

Model Values	CAPE	TT	KI	Model to Model	TT	KI
A	61	47	26	A to B	6.8	0
	310	48	26		4.3	18.2
	536	49	32		8.9	14.3
	0	33	14		15.4	17.6
	0	36	−1		5.3	120.0
	0	34	−7		0	0
	0	34	2		2.9	60
B	0	44	26	B to C	6.4	4.0
	90	46	22		4.2	12.0
	357	45	28		8.2	0
	0	39	17		14.7	13.3
	0	38	5		1.8	600.0
	0	34	−7		0	0
	0	35	5		0	28.6
C	9	47	25	A to C	0	4.0
	254	48	25		0	4.0
	536	49	28		0	14.3
	0	34	15		2.9	6.7
	0	34	−1		5.9	0
	0	34	−7		0	0
	0	35	7		2.9	71.4
WRF	−	25	−14	A to WRF	46.8	153.8
	−	26	−19		45.8	173.1
	−	29	−16		40.8	150.0
	−	29	−5		12.1	135.7
	−	29	−4		19.4	300.0
	−	36	7		5.9	200.0
	−	35	3		2.9	50.0
				B to WRF	76.0	160.9
					43.5	186.4
					35.6	157.1
					25.6	129.4
					23.7	180.0
					5.9	200.0
					0	40.0
				C to WRF	88.0	156.0
					45.8	176.0
					40.8	157.1
					14.7	133.3
					14.7	300.0
					5.9	200.0
					0	57.1

Table 3. As in Table 2, except for KFWD.

Model Values	CAPE	TT	KI	Model-to-Model	TT	KI
A	129	40	30	A to B	2.6	3.4
	149	40	20		5.3	9.1
	6	40	24		11.1	14.3
	0	23	−17		0.0	41.7
	0	34	3		3.0	200.0
	0	39	3		2.6	200.0
	0	36	2		0.0	100.0
B	128	39	29	B to C	0.0	3.6
	329	40	22		5.3	10.0
	60	41	21		13.9	133.3
	0	25	−12		8.7	14.3
	0	32	1		3.0	75.0
	0	37	1		2.6	50.0
	0	36	1		0.0	50.0
C	80	39	28	A to C	2.6	7.1
	121	38	20		5.3	0.0
	0	36	9		11.1	166.7
	0	23	−14		0.0	21.4
	0	33	4		3.0	25.0
	0	38	2		2.6	50.0
	0	36	2		0.0	0.0
WRF	–	33	2	A to WRF	21.2	93.3
	–	36	7		10.0	65.0
	–	39	7		2.5	70.8
	–	40	−1		73.9	94.1
	–	36	−6		5.9	300.0
	–	39	−6		0.0	300.0
					0.0	300.0
				B to WRF	18.2	93.1
					10.0	68.2
					4.9	66.7
					60.0	91.7
					12.5	700.0
					5.4	700.0
					0.0	500.0
				C to WRF	18.2	92.9
					5.3	65.0
					8.3	22.2
					73.9	92.9
					9.1	250.0
					2.6	400.0
					0.0	300.0

Table 4. As in Table 2, except for KBNA.

Model Values	CAPE	TT	KI	Model-to-Model	TT	KI
A	0	41	27	A to B	5.1	8.0
	56	34	24		0.0	4.3
	33	40	28		5.3	7.7
	0	39	32		7.1	0.0
	98	44	23		2.3	28.1
	215	44	34		10.0	13.3
	35	35	2		2.8	86.7
B	0	39	25	B to C	4.9	7.4
	2	34	23		0	4.2
	0	38	26		2.6	0
	0	42	32		10.5	3.2
	130	43	32		0	0.0
	122	40	30		13.0	16.7
	7	36	15		7.7	87.5
C	0	41	27	A to C	0	0
	11	34	24		0	0
	5	39	26		2.6	7.7
	12	38	31		2.6	3.2
	322	43	32		2.3	28.1
	0	46	36		4.3	5.6
	217	39	8		10.3	75.0
WRF	–	45	21	A to WRF	8.9	22.2
	–	47	22		38.2	8.3
	–	48	20		20.0	28.6
	–	47	24		20.5	25.0
	–	48	27		9.1	17.4
	–	45	25		2.3	226.5
	–	46	21		31.4	950.0
				B to WRF	13.3	16.0
					38.2	4.3
					26.3	23.1
					11.9	25.0
					11.6	15.6
					12.5	16.7
					27.8	40.0
				C to WRF	8.9	22.2
					38.2	8.3
					23.1	23.1
					23.7	22.6
					11.6	15.6
					2.2	30.6
					17.9	162.5

BNA had the fewest differences through the entire run, although the differences at ILN would be lower if the error for the first time period is dropped. These errors showed a large percent difference due to the values being very small. KFWD had significant differences after 00Z 27 October. Differences in the TT remained below 15% for all locations in the MASS-A to

MASS-C comparison. KFWD, KBNA, and KILN showed differences initially but KBNA and KILN showed greater differences between 1800 UTC 27 October and 0000 UTC 28 October. KILN had the fewest differences in KI for the entire duration after the initial time. Both KTOP and KBNA had high differences at 0000 UTC 28 October. The MASS-B to MASS-C

Table 5. As in Table 2, except for KILN.

Model Values	CAPE	TT	KI	Model-to-Model	TT	KI
A	0	21	2	A to B	0	0
	0	32	16		0	0
	0	35	21		9.4	10.5
	0	31	17		0	5.6
	213	33	20		3.1	0
	0	37	25		2.8	0
	0	35	24		12.5	14.3
B	0	21	2	B to C	0	0
	0	32	16		0	0
	29	32	19		8.6	9.5
	52	31	18		6.1	0
	0	32	20		11.1	4.8
	0	36	25		2.7	3.8
	84	40	28		2.4	3.7
C	0	21	2	A to C	0.0	0.0
	0	32	16		0.0	0.0
	0	35	21		0.0	0.0
	0	33	18		6.1	5.6
	89	36	21		8.3	4.8
	0	37	26		0.0	3.8
	2	41	27		14.6	11.1
WRF	–	42	29	A to WRF	50.0	1350.0
	–	43	30		34.4	87.5
	–	41	28		17.1	33.3
	–	42	28		35.5	64.7
	–	43	30		30.3	50.0
	–	41	28		10.8	12.0
	–	41	28		17.1	16.7
				B to WRF	50.0	1350.0
					34.4	87.5
					28.1	47.4
					35.5	55.6
					34.4	50.0
					13.9	12.0
					2.5	0.0
				C to WRF	50.0	1350.0
					34.4	87.5
					17.1	33.3
					27.3	55.6
					19.4	42.9
					10.8	7.7
					0.0	3.7

comparison showed that more errors differences in the TT between the 0600 UTC and 1200 UTC 27 October. Differences were generally below 15% overall. KFWD had significant differences for most of the duration for KI, BNA had the least. At 0000 UTC 28 October, there were large differences in KI for KTOP, KBNA, and KFWD. Overall KBNA had the lowest differences in the intermodel and intramodel comparisons.

Operational Forecasting Implications

While the goal of this work was not to focus on the superiority of a particular model or parameterization, there are nonetheless some implications that can be drawn from this study. It is not surprising to the forecaster to know that model-to-model differences frequently occur even in short term forecasts. However, even small differences between models in the 500 hPa height and temperature fields, which may seem unimportant, can yield very different impressions regarding the likelihood and type of precipitation that may be predicted. This shows the difficulties that a forecaster can have in attempting to determine the type and amount of precipitation that could fall over a region. Additionally, the intra-model differences were larger than the differences within the MASS model due to differences in the convective paramterizations. While it is not common practice to use different models in an ensemble for the same event, this work implies that doing so may provide more useful results than the current practice of simply varying the initial conditions.

Also, the calculation of the Lyapunov time-scale using 500 hPa heights yielded a time-scale for predictability that was consistent with that predicted by theory and a subjective analysis of the reliability of the convective precipitation predictions. Thus, as implied by the use of empirical indexes in previous decades, large-scale information can be a useful guide for the reliability of the forecasts of mesoscale features.

Summary and Conclusions

Using observational data along with model predictions from the GFS, MASS and WRF, the practical meaning of the sensitive dependence on the initial conditions and the chaotic behavior of atmosphere can be demonstrated, as well as the implications for the reliability of model forecasts. It was shown that the Dymnikov [4] method for determining the degree of predictability used here can be effective [24] [25] and used in an operational environment, which has not been shown before in the literature. It was determined that the GFS and MASS models exhibit chaotic behavior especially at and beyond approximately 36 hours. These calculations agree with results calculated from a theoretical perspective and the model observations regarding the convective precipitation forecast.

Determining the difference among each scheme of the MASS and the WRF qualitatively provides benefits to the observer. The differences between each model run could lead the forecaster to make a decision between what kind of precipitation event might be forecast (e.g. convective versus stratiform, or precipitation type). Finding the areas where the models did not agree allowed the focus in this study to be centered on calculating the exact degree of the differences between the convective stability indexes.

The comparison between the intramodel and intermodel differences in the indexes revealed that the MASS-A and

Figure 5. The mean percent differences for a) KTOP, b) KFWD, c) KBNA, and d) KILN versus the model-to-model comparisons found in Tables 2–5.
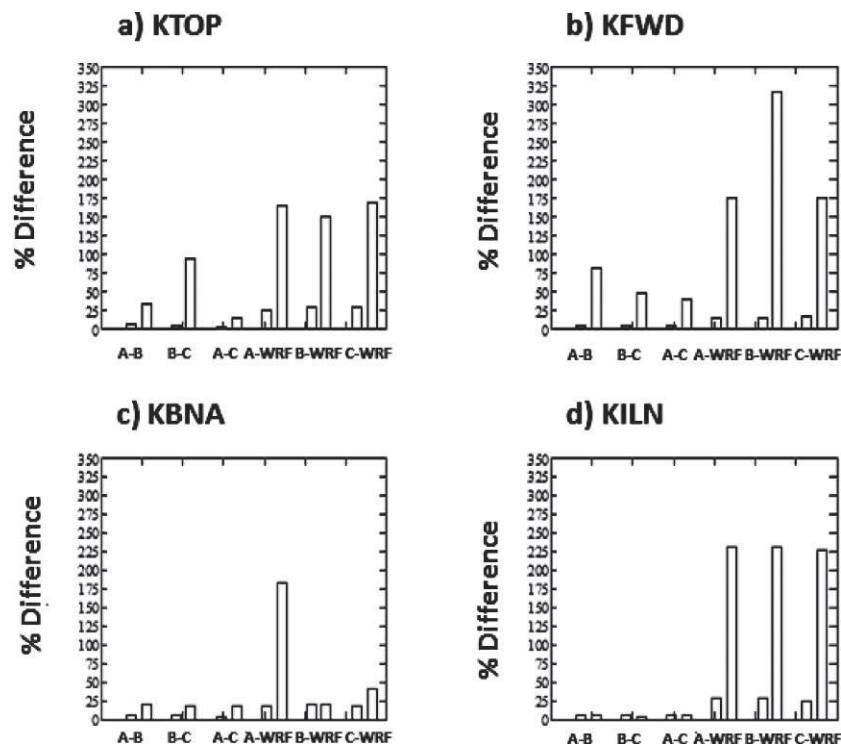
MASS-C were the best when using both TT and KI. We could not find this kind of comparative study in the literature for stability. Generally, studies look at differences between primary variables. Differences were relatively low for the entire duration of the forecast period at all locations. When either model was compared to B, larger differences occurred. A comparison to the WRF model revealed that the MASS (WRF) model produced stronger (weaker) TTs downstream (upstream) of the developing cyclone of late October 2006.

Generally, the TT had lower difference values than KI between each scheme of the MASS and between WRF and each MASS scheme. Differences between each scheme and the WRF were altogether poor when using KI. The initial values were very high and not much better at 0000 UTC 28 October. Using the TT, model C had the best resolution even though it had the highest initial differences. Finally, the differences in the model forecasts between convective parameterizations (intramodel forecasts) in this case were not as great as the model-to-model forecast differences (intermodel forecasts). It is not common practice to create forecast ensembles using different models, however, this work suggests that the practice may provide more useful information in an operational environment.

References

1. E. Lorenz, "Three approaches to atmospheric predictability", *Bull. Amer. Meteor Soc*, vol. 50, pp. 345–349, 1969.
2. S.M. Griffes, and K. Bryan, "A predictability study of simulated North Atlantic multidecadal variability". *Climate Dynamics*, vol. 13, pp. 459–487, 1997.
3. A.M. Lyapunov, "Stability of motion". *Academic Press*, 1966.
4. V.P. Dymnikov, E.V Kazantsev, and V.V. Kharin. "Informational entropy and local Lyapunov exponents of barotropic atmospheric circulation*" Izvestia, Atmospheric and Oceanic Physics*, vol. 28, No 6, pp. 563–573, 1992.
5. R.A. Cohen, and D.M. Schultz, "Contraction rate and it's relationship to frontogenesis, the Lyapunov exponent, fluid trapping, and air stream boundaries". *Mon. Wea. Rev.*, vol. 133, pp. 1353–1369, 2005.
6. R.C. Bishop, "On the separability of prediction and determinism". *Erkenntnis*, vol. 58, pp. 169–188, 2003.
7. F. Zhang, C. Snyder, and R. Rotunno, "Effects of moist convection on mesoscale predictability", *J. Atmos. Sci.*, vol. 60, pp. 1173–1185, 2003.

8. Z.M. Tan, F. Zhang, R. Rotunno, and C. Snyder, "Mesoscale predictability of moist baroclinic waves: Experiments with parameterized convection", *J. Atmos. Sci.*, vol. 61, pp. 1794–1804, 2004.

9. J.S. Kain, "The Kain-Fritsch convective parameterization: An update", *J. Appl. Meteor.*, vol. 43, pp. 170–181, 2004.

10. G.A. Grell, and D. Devenyi, "Parameterized convection with ensemble closure/feedback assumptions", *Preprints, 9th Conf. on Mesoscale Processes, Fort Lauderdale, FL*, *Amer. Meteor. Soc.*, pp. 12–16, 2001.

11. G.A. Grell, and D. Devenyi, "A generalized approach to parameterizing convection combining ensemble and data assimilation techniques", *Geoph. Res. Letters*, vol. 29, no. 14, doi 10.1029/2002GL015311, 2002.

12. Z.I. Janjic, "The step-mountain Eta coordinate model: Further developments of the convection, viscous sublayer, and turbulence closure schemes. *Mon. Wea. Rev.*, vol. 122, pp. 927–945, 1994.

13. S.S. Vaidva and S.S. Singh, "Applying the Betts-Miller-Janjic Scheme of convection in prediction of the Indian Monsoon. *Wea. Fcsting*, vol. 15, pp. 349–356, 2000.

14. A.R. Lupo, P.J. Smith, and P. Zwack, "A Diagnosis of the Development of Two Extratropical Cyclones", *Mon. Wea. Rev.*, vol. 120, pp. 1490–1523, 1992.

15. J. Sela, "Spectral modeling at the National Meteorological Center," *Mon. Wea. Rev.* vol. 108, pp. 1279–1292, 1980.

16. Z. Toth, and E. Kalnay, "Ensemble forecasting at NCEP: The generation of perturbations", *Bull Amer. Meteor. Soc.*, vol. 74, pp. 2317–2330, 1993.

17. Z. Toth, Z., and E.. Kalnay, "Ensemble forecasting at NCEP and the breeding method", *Mon. Wea. Rev.*, vol. 125, pp. 3297–3319, 1997.

18. M.S. Tracton, and E. Kalnay, "Ensemble forecasting at the National Meteorological Center: Practical Aspects", *Wea. and Forecasting*, vol. 8, pp. 379–398, 1993.

19. I. Szunyogh, and Z. Toth, "The effect of increased horizontal resolution on the NCEP global ensemble mean forecasts", *Mon. Wea. Rev.*, vol. 130, pp. 1125–1143, 2002.

20. J. Manobianco, J. W. Zack, and G.E. Taylor, "Workstation-based real-time mesoscale modeling designed for weather support to operations at the Kennedy Space Center and Cape Canaveral Air Station", *Bull Amer Meteor. Soc.*, vol. 77, pp. 653–672, 1996

21. Y.L. Lin, R. D. Farley, and H. D. Orville, "Bulk parameterization of the snow field in a cloud model", *J. Climate Appl. Meteor.*, vol. 22, pp. 1065–1092, 1983.

22. J.S. Sturtevant, "The Severe Local Storm Forecasting Primer", 197 pp., 1995.

23. A.R. Lupo, I.I. Mokhov, S. Dostoglou, A.R. Kunz, and J. P. Burkhardt, "The impact of the planetary scale on the decay of blocking and the use of phase diagrams and enstrophy as a diagnostic", *Izvestiya, Atms-Oc.*, vol. 43, pp. 45–51, 2007.

24. A. Hussain, and A.R. Lupo, "Scale and stability analysis of blocking events from 2002–2004: A case study of an unusually persistent blocking event leading to a heat wave in the Gulf of Alaska during August 2004", *Adv. Meteor.* vol. 2010, Article ID 610263, 15 pages doi:10.1155/2010/610263, 2010.

25. A.R. Lupo, I.I. Mokhov, M.G. Akperov, A.V. Chernokulsky, and H. Athar, "A dynamic analysis of the role of the planetary- and synoptic-scale in the summer of 2010 blocking episodes over the European part of Russia", *Adv. Meteor.*, vol. 2012, Article ID 584257, 11 pages, doi:10.1155/2012/584257, 2012.

26. W.E. Boyce, and R.C DiPrima, "Elementary Differential Equations and Boundary Value Problems, 4th Ed.", John Wiley and Sons, 640 pp., 1986.

27. S. Businger, M.E. Adams, S.E. Koch, M.L. Kaplan, "Extraction of Geopotential Height and Temperature Structure from Profiler and Rawinsonde Winds", *Mon. Wea. Rev.*, vol. 129, pp. 1729–1739, 2001.